Chemical Science

ROYAL SOCIETY OF CHEMISTRY

EDGE ARTICLE

View Article Online
View Journal | View Issue

Cite this: *Chem. Sci.*, 2025, **16**, 18211

All publication charges for this article have been paid for by the Royal Society of Chemistry

Received 24th April 2025
Accepted 1st September 2025

DOI: 10.1039/d5sc03012a

rsc.li/chemical-science

Optimizing semi-hydrogenation of unsaturated hydrocarbons by electrolyte engineering approach

Rongyu Zhang, [a] Xingyi Lyu, [b] Tao Li [bc] and Alexis Grimaud *[a]

Electrochemical hydrogenation of unsaturated hydrocarbons, when powered by renewables, represents a unique opportunity to substitute current energy-intensive synthetic routes. Modulation of adsorption energies of the organic substrate and key intermediates of the reaction is critical for fine tuning of the yield, selectivity and kinetics of the reaction. Interestingly, mounting evidence exists regarding the role of electrolyte composition in the outcome of semi-hydrogenation reactions. Nevertheless, electrolyte optimization is a complex task, owing to its hybrid nature. Indeed, it is composed of water serving as a proton source, an organic solvent necessary to dissolve the organic substrate and a conducting salt. Herein, we demonstrate that varying conducting salt and organic solvent has a dramatic impact on the outcomes of semi-hydrogenation of alkynes. By varying salt and water concentrations, we demonstrate that water does not serve as a proton source, and instead addition of an acid is necessary. While increasing the acid concentration increases the yield of the reaction, at too large concentrations the hydrogen evolution reaction becomes predominant. Furthermore, by combining electrochemical measurements with spectroscopic techniques including Fourier transform infrared (FTIR) spectroscopy and small angle X-ray spectroscopy (SAXS), we demonstrate that the electrolyte solvation structure dramatically impacts the yield of the reaction. Organic solvents weakly interacting with water, including acetonitrile, form aqueous nanoheterogeneities that prevent the organic substrate from accessing the catalyst interface and thus lead to limited yields. Instead, solvents such as dimethylformamide form homogeneous mixtures with which all reactants can access the interface, leading to yields greater than 80% for optimized compositions.

Introduction

Organic electrosynthesis has recently gained renewed attention as, when powered by renewables, it is regarded as a more environmentally friendly approach compared to energy-intensive routes utilizing redox reagents.[1–4] This is specifically the case for hydrogenation reactions, for which conventional synthesis routes require harsh conditions,[5] including high temperature[6] or high pressure,[7,8] and complex procedures to achieve good yield and conversion. So far, a variety of electrosynthesis strategies have been developed and employed for efficient and selective hydrogenation of unsaturated organic compounds.[9–14] Most efforts have been devoted to designing better electrocatalysts with the aim of enhancing the reaction rate and selectivity by controlling the intermediates forming on the surface of the catalyst.[12,15,16] Nevertheless, numerous results point to the critical role played by electrolyte optimization on the outcome of hydrogenation reactions, more specifically its composition.[17,18]

As commonly believed, hydrogenation reactions require the formation of H* intermediates following the electrochemical reduction of water or protons, with these intermediates being transferred to the unsaturated hydrocarbon (alkyne or alkene) or involved in a hydration–dehalogenation process.[10,19–21] Nevertheless, when targeting the hydration of insoluble organic substrates, water that acts as a proton source must be mixed with an organic solvent to solubilize the organic substrate, forming a so-called hybrid electrolyte.[22] Hybrid electrolytes have thus been used in various hydrogenation reactions, including the semi-hydrogenation of alkynes into alkenes or the hydrogenation of halogenated alkyls, using solvents including acetonitrile (ACN), dimethylformamide (DMF), or acetone, among others.[23–25]

Past studies have shown that the composition and structure of hybrid electrolytes strongly impact the water reactivity at electrochemical interface, with the hydrogen evolution reaction (HER) competing with hydrogenation reactions in hybrid electrolytes being highly sensitive to the organic solvent.[26,27] This effect is rooted in the role played by short-range interactions, including ion–water, water–water and organic solvent–water,

[a]*Department of Chemistry, Boston College, Chestnut Hill, MA, 02467, USA. E-mail: alexis.grimaud@bc.edu*

[b]*Department of Chemistry and Biochemistry, Northern Illinois University, DeKalb, IL, 60115, USA*

[c]*X-ray Science Division, Argonne National Laboratory, Lemont, IL, 60439, USA*

which drastically modify the solvation structure and the dynamics of hybrid electrolytes.[22,27,28] Hence, when the organic solvent strongly interacts with water, small angle X-ray scattering spectroscopy (SAXS) coupled with molecular dynamics (MD) simulation showed that water and organic molecules are homogeneously dispersed in the hybrid electrolyte, as observed for DMF/water mixtures.[29–32] In contrast, when the organic solvent only weakly interacts with water, aqueous and organic nanodomains co-exist in the mixtures, such as for ACN/water mixtures.[28,33–37] As recently reported, the size and composition of these nanodomains can affect the selectivity and efficiency of electrochemical reactions,[27] including the HER or CO_2 reduction.[22,38] Similarly, the strength of the water–cation interactions was found to affect the solvation structure of these hybrid electrolytes and the selectivity of electrocatalytic reactions.[27,28]

Despite being well documented, efforts dedicated to the optimization of the reaction micro-environment, *i.e.* the liquid electrolyte composition and solvation structure, remain sparse. More specifically, the effect of water heterogeneities, their size and composition, on the outcome of electrochemical hydrogenation of unsaturated hydrocarbons remains poorly understood. In this work, we investigate how the structure of hybrid organic solvent/water electrolytes impacts the competition between the HER and electrochemical organic hydrogenation. To probe this effect, the selective hydrogenation of diphenylacetylene into *Z*-stilbene is studied as a model reaction,[19,20] diphenylacetylene being directly reduced at more negative potentials than water. To control the formation of aqueous heterogeneities, three organic solvents, ACN, acetone, and DMF, were selected with varying strengths of interaction with water, from strong to weak, following DMF > acetone > ACN. Similarly, the proton source is varied from water to sulfuric acid. The formation of water clusters in the hybrid solution is characterized by combining Fourier transform infrared (FTIR) spectroscopy and synchrotron SAXS. Our results demonstrate that heterogeneities play a critical role in the outcome of the reaction, with yields greater than 80% obtained with optimized compositions. Even though the aqueous heterogeneities in ACN-based electrolyte can be modified by varying the amount of acids or solvents, the outcome of semihydrogenation stays low. In contrast, we find the optimum yield in DMF- and acetone-based electrolytes, showing the pivotal role of the reaction environment in electrochemical semi-hydrogenation. Finally, we demonstrate that these findings are common to less oleophilic alkynes, including phenylacetylene, and to aldehydes which are prone to compete with the organic solvent for interacting with water.

Results and discussion

Prior to studying the effect of the solvation structure on the outcome of the semi-hydrogenation of diphenylacetylene, one must first recall that water/DMF mixtures possess a negative excess enthalpy for mixing (ΔH_{mix}), indicating strong interactions between water and DMF.[27] Instead, ΔH_{mix} for water/ACN mixtures is positive, owing to the weak interactions between ACN and water molecules. Water/acetone mixtures possess a slightly positive ΔH_{mix} at low molar fractions of water, while it is negative at large molar fractions of water (>0.5), as those studied in this work. Electrochemical study shows that this difference in strength of interaction shifts the HER potential (at a current density of -2 mA cm^{-2}) on the surface of a Pt electrode towards more negative values following ACN (-1.626 V *vs.* RHE) > acetone (-1.689 V *vs.* RHE) > DMF (-1.995 V *vs.* RHE) (Fig. S1a), in line with our previous observations.[27] Furthermore, increasing the concentration of $LiClO_4$ from 0.1 to 1 M was found to increase the kinetics for the HER, *i.e.* to induce a shift towards more positive potential (Fig. S1b), likely as a result of a facilitated water dissociation step;[22,39,40] this effect is observed independently of the water-organic solvent interaction strength.

When adding diphenylacetylene in hybrid electrolytes containing ACN, acetone, or DMF with 5 M H_2O and different concentrations of $LiClO_4$, only traces of the product were detected after 2 hours of electrolysis at -0.8 V *vs.* Ag/AgCl at room temperature. This finding indicates that either water does not act as a proton source for hydrogenation under these conditions and/or that the HER is too fast on the surface of Pt. To disentangle both effects, similar experiments were carried out using Ni foam electrodes, previously reported to be an efficient hydrogenation electrocatalyst,[19] and no product was detected for the three solvents (Fig. S6), confirming that water does not act as a proton source.

Having established that water does not serve as a proton source for the semihydrogenation reaction in hybrid electrolytes, yields were measured after 2 hours of electrolysis at -0.8 V *vs.* Ag/AgCl in $HClO_4/H_2O$/organic solvent mixtures, and the results are plotted for different acid concentrations and organic solvents in Fig. 1b. In ACN/water mixtures (1 : 1, v/v), the yield is found to be independent of acid concentrations and much lower than that for other mixtures. By quantifying all the products formed during hydrogenation of diphenylacetylene, including both isomers formed by semihydrogenation (*cis*- and *trans*-stilbene) and dibenzyl formed by overhydrogenation, we conclude that the low conversion observed in ACN mixtures is not due to a favored overhydrogenation, the preferred formation of the second isomer (Table 1), or any other side reactions (Table S3). Fixing the applied potential to -1.1 V *vs.* RHE during the hydrogenation in 1.5 M $HClO_4/H_2O$/solvent mixtures, similar results were obtained, ruling out any effect of difference in the overpotential on this process (Table S2). Moreover, the results gathered using a Ni foam were compared with those obtained with polished Ni foil under the same conditions (1.5 M $HClO_4$ H_2O/solvent mixtures at -0.8 V *vs.* Ag/AgCl for 2 hours). While lower yields were obtained due to the smaller active surface area (as determined in Fig. S16), a similar trend to the one obtained with the Ni foam was observed (Fig. S3a), excluding the effect from wettability, pores access or mass transport to explain the difference measured between these three solvents.[41]

For acetone/water (1 : 1, v/v) and DMF/water (1 : 1, v/v) mixtures, the yield first increases with acid concentration before decreasing. To comprehend this trend, cyclic voltammograms were recorded to estimate the HER potential in these

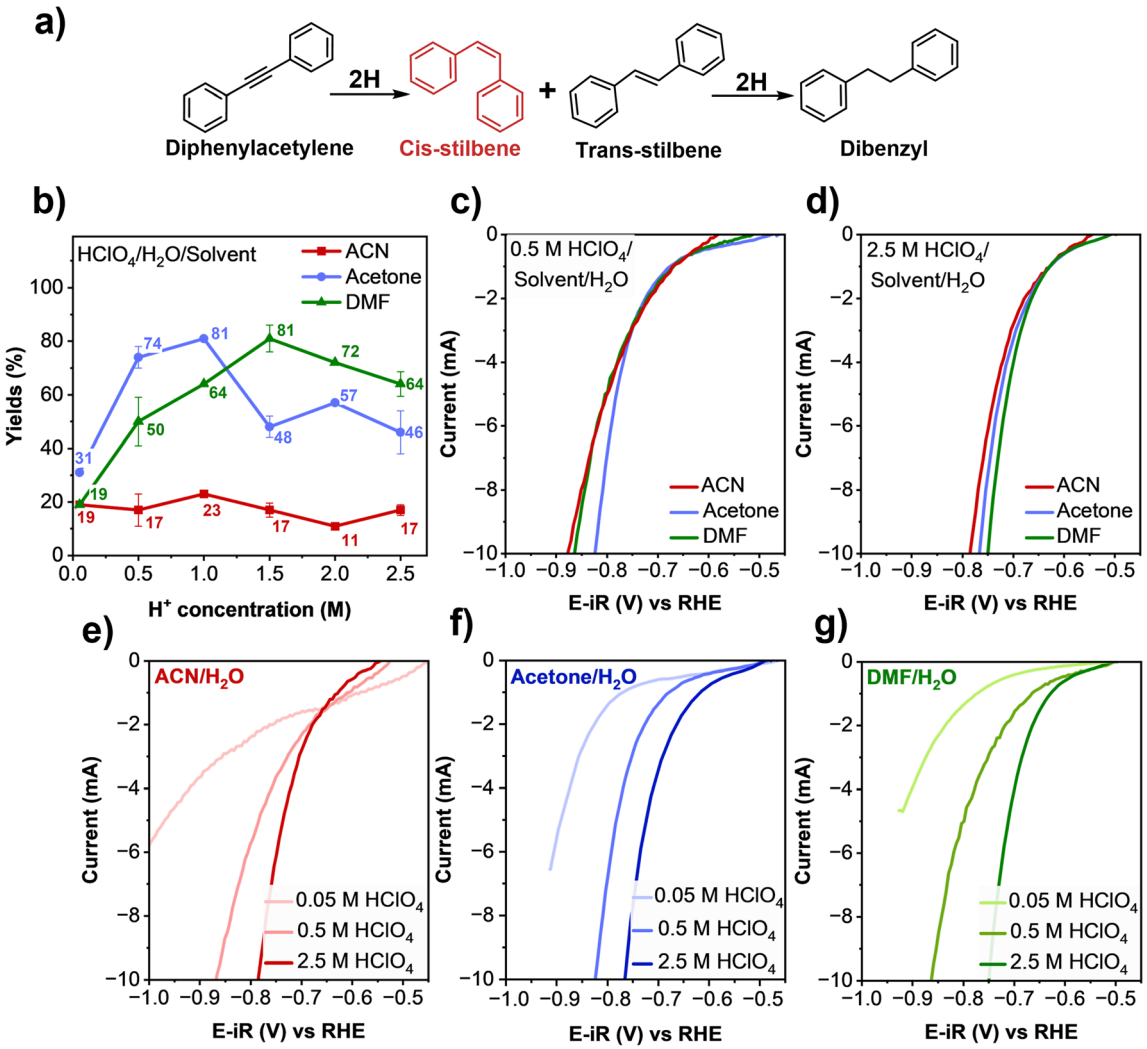

Fig. 1 (a) The hydrogenation processes of diphenylacetylene. (b) Yields measured in hybrid electrolytes with different $HClO_4$ concentrations and organic solvents after 2 hours of electrolysis at −0.8 V *vs.* Ag/AgCl. (c) and (d) Cyclic voltammograms recorded for hybrid electrolytes containing 0.5 M and 2.5 M $HClO_4$, respectively. (e)–(g) Cyclic voltammograms recorded for different $HClO_4$ concentrations in H_2O and ACN, acetone, and DMF hybrid electrolytes, respectively.

mixtures against the reversible hydrogen electrode (RHE) which was estimated in each solution (see Experimental section). When the acid concentration is fixed, the HER potential is similar in ACN-, acetone-, and DMF-based mixtures (Fig. 1c and d). This absence of shift is due to the fast reduction of protons when compared to water.[42–46] Proton reduction is thus not sensitive to the organic solvent, unlike water reduction for which the water dissociation step depends on the strength of the solvent molecules–water interactions. Nevertheless, the HER potential shifts to less negative potentials with higher acid

Table 1 Hydrogenation products in hybrid electrolytes at −0.8 V *vs.* Ag/AgCl for 2 hours

	Selectivity (%)			
	Cis-stilbene	Trans-stilbene	Dibenzyl	
Hybrid electrolytes				Conversion (%)
1.5 M $HClO_4/H_2O$/DMF	84	2.3	8.3	94.6
1.5 M $HClO_4/H_2O$/acetone	51	12.6	26	89.6
1.5 M $HClO_4/H_2O$/ACN	14	0.8	0.6	15.4

concentrations (see Fig. 1e–g and HER overpotential listed in Table S1). We therefore attribute the maximum yield observed in acetone/water and DMF/water mixtures when a fixed potential is applied *vs.* Ag/AgCl, respectively, at 1 M and 1.5 M of $HClO_4$, to the shift of the HER overpotential with acid concentration.[27] When increasing the acid concentration, the HER becomes faster and dominates over the semihydrogenation reaction. Finally, and not surprisingly, the yield of semihydrogenation is found to decrease when the applied potential is decreased in 1.5 M $HClO_4$ DMF/water electrolyte (Fig. S2), indicating that the kinetics for the semihydrogenation are dependent on potential, like in the HER.

To further confirm the trend, the reaction was carried out in a proton membrane reactor, typically used in electrochemical hydrogenation,[47–49] using the optimal reaction conditions as found above (1.5 M $HClO_4/H_2O$/solvent electrolytes and a fixed applied potential of −0.8 V *vs.* Ag/AgCl for 2 hours). When comparing the results obtained in three electrode configuration and those obtained using a proton membrane reactor, similar trends are observed with the semihydrogenation yields in ACN mixtures being very low while those in acetone and DMF mixtures are much greater; one must however note that the yield recorded in DMF mixtures is slightly lower in the proton membrane reactor than that in the three electrode configuration (Fig. S3b). We thus conclude that these differences do not arise from extrinsic factors related to cell design.

Having established the impact of solvent, acid concentration and applied potential on the yield of semihydrogenation, we then turned our attention to the effect of water content by varying the organic solvent to water volume ratio from 1 : 1 to 5 : 1 (Fig. 2a). For all the hybrid electrolytes tested in this work, the yield increases with the amount of water. This variation is not explained by a change in the HER kinetics, which remains constant in these hybrid electrolytes when varying the organic solvents or the ratio of solvent/water (Fig. 2b, c and S8). This result indicates that the HER remains faster than the hydrogenation under these conditions and that proton reduction is not affected when varying the organic solvent/water ratio (Fig. S8). Observing that water remains in large excess compared to diphenylacetylene in all the mixtures, we hypothesize that the semi-hydrogenation reaction is limited by the transport of diphenylacetylene to the interface (see the discussion below). Finally, we confirmed that semi-hydrogenation is insensitive to electrolyte anions by comparing the yields obtained in perchloric and sulfuric acids, with the latter known to block the active sites for the HER. Indeed, the HER potentials are found to be shifted to more negative potentials on the Ni electrode in hybrid electrolytes containing sulfuric acid (Fig. S9b–i). Instead, for all mixtures, switching to sulfuric acid does not affect the yields when using the Ni electrode (Fig. S9a). This difference in reactivity may indicate that the HER and the hydrogenation reaction do not share similar intermediates and/or reaction mechanisms, as suggested in studies proposing that hydrogenation follows an outer-sphere reduction–protonation mechanism or an Eley–Rideal type mechanism that differs from the Volmer–Heyrovsky or Volmer–Tafel HER mechanism.[50] Nevertheless, as seen in Fig. S10, the cathodic current recorded using Ni foam experiences a significant shift towards more negative potential when adding diphenylacetylene in the various mixtures, which may indicate the adsorption of the substrate at the electrode. Further work, including using surface enhanced spectroscopy techniques or computational chemistry with explicit solvent and applied potential, will be needed to clarify the exact semihydrogenation mechanism in these hybrid mixtures.

The trend observed with diphenylacetylene is also observed for the hydrogenation of other substrates, knowing that diphenylacetylene is an extremely oleophilic unsaturated organic substrate that shows very weak interaction with water. For this goal, we selected two other substrates, including another alkyne, phenylacetylene, and an aldehyde (benzaldehyde) that likely shows different interactions with water. Hydrogenation reactions were conducted in the different 1.5 M $HClO_4/H_2O$/solvent electrolytes. The outcome of the phenylacetylene hydrogenation was found to be similar to that of the bulkier diphenylacetylene, with acetone and DMF providing higher

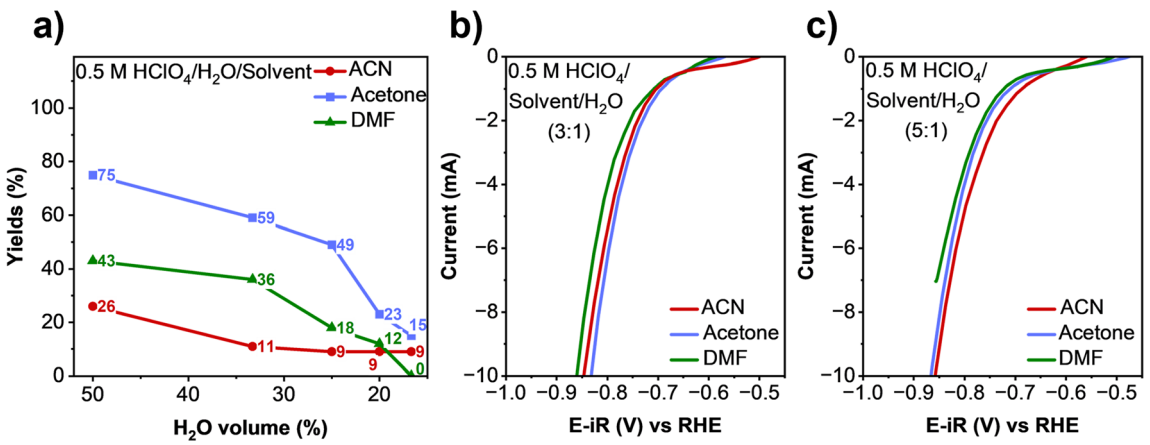

Fig. 2 (a) Yields in the 0.5 M $HClO_4$ hybrid electrolytes with different H_2O and organic solvent compositions. (b) and (c) Cyclic voltammograms recorded for hybrid electrolytes containing 0.5 M $HClO_4$ with different H_2O and organic solvent compositions.

yields than ACN for the semihydrogenation product (styrene), while some overhydrogenation product (ethylbenzene) was found in the various mixtures as phenylacetylene is easier to over-reduce when compared to diphenylacetylene (Fig. 3a). For benzaldehyde, ACN again showed a significantly lower yield for the formation of the semihydrogenation product (benzyl alcohol) (Fig. 3b). However, significantly higher yield was observed in acetone mixtures compared to DMF which may be attributed to the chemical similarities existing between benzaldehyde and acetone and their comparable ability to form hydrogen bonding with water that was previously shown to be critical for increasing the hydrogenation reaction.[51,52]

One observation remains thus far unexplained: the effect of solvent on the semi-hydrogenation reaction, with the yields found to increase with its strength of interaction with water. To investigate the impact of local heterogeneities on the semi-hydrogenation reaction, we turned to SAXS measurements. SAXS patterns were measured with different $HClO_4$ concentrations in the q range of 0.02 to 1.2 $Å^{-1}$ (Fig. 4), where the 0.02 to 0.6 $Å^{-1}$ q range corresponding to distances of 10.4 to 314.2 Å ($2\pi/q$) contains information regarding the growth of aqueous heterogeneities in hybrid electrolytes.[53,54] The SAXS patterns of ACN/water mixtures show a characteristic shape (Fig. 4a and b), with scattering intensity observed in this low q range indicating the formation of water clusters in the mixtures owing to H_2O–H_2O and ACN–ACN self-correlation.[27,55] Meanwhile, a relatively weak bump indicates that the heterogeneity in the acetone/water mixture is less pronounced compared to that in the ACN/water system. In contrast, the SAXS profile of the DMF/water mixture nearly overlaps with that of pure water, suggesting a high degree of miscibility between DMF and water. When increasing the acid concentration, the scattering intensity drops and the Guinier region shifts to the high q region, indicating a reduction in both the size and the amount of the clusters. This finding is opposite to that previously observed for strong Lewis acids such as Li^+, for which increasing the concentration was found to increase the size of the heterogeneities, owing to the strong Li^+–H_2O interactions.[22] In contrast, as shown in Fig. 4d–g, the solvation structure of acetone/water mixtures and DMF/water mixtures is independent of the amount of $HClO_4$ concentration and the water to organic solvent volume ratio. These SAXS results confirm that, as previously observed in $LiClO_4$-containing mixtures, little to no heterogeneity forms in $HClO_4$-containing acetone/water and DMF/water hybrid solution owing to the strong organic solvent–water interactions. Conversely, the heterogeneities that are formed in ACN/water mixtures and their size are highly sensitive to the acid concentration. Here, our results highlight that protons disrupt the hydrogen bonding network (Fig. 4c). This conclusion is confirmed by observing that the scattering intensity decreases when decreasing the amount of water from 1 : 1 to 5 : 1 (v/v).

The SAXS results were complemented by FTIR measurements to gain more insights into the water environment in these mixtures (Fig. 5a–c). Looking into the OH stretching region (2800–3700 cm^{-1} range), a band composed of several components is observed. From previous results, one can tentatively assign the different components to isolated water molecules (~3620 cm^{-1}), one or two H-bonded water molecules (~3540 cm^{-1}), ice-like distorted tetrahedral water networks (~3420 cm^{-1}) and ice-like water networks (~3250 cm^{-1}) (Fig. 4g).[56–58] From IR spectra collected in solvent/water mixtures at different $HClO_4$ concentrations, the intensity of the contributions at ~3420 cm^{-1} and ~3250 cm^{-1} decreases in all mixtures with the addition of $HClO_4$, indicating the breaking of the hydrogen bonding networks. This is accompanied by an increase in intensity for the contribution at ~3620 cm^{-1}, indicating weaker hydrogen bonding.[56] Therefore, we conclude that protons are preferentially interacting with water molecules in these electrolytes, destabilizing the water–water interactions. This hypothesis is supported by observing that increasing the solvent to water volume ratio from 1 : 1 to 5 : 1 (Fig. 5d–f), *i.e.* decreasing the water–water interactions, decreases the intensity of the OH stretching bands in all mixtures. More precisely, the features at low wavenumbers dramatically decrease, indicating

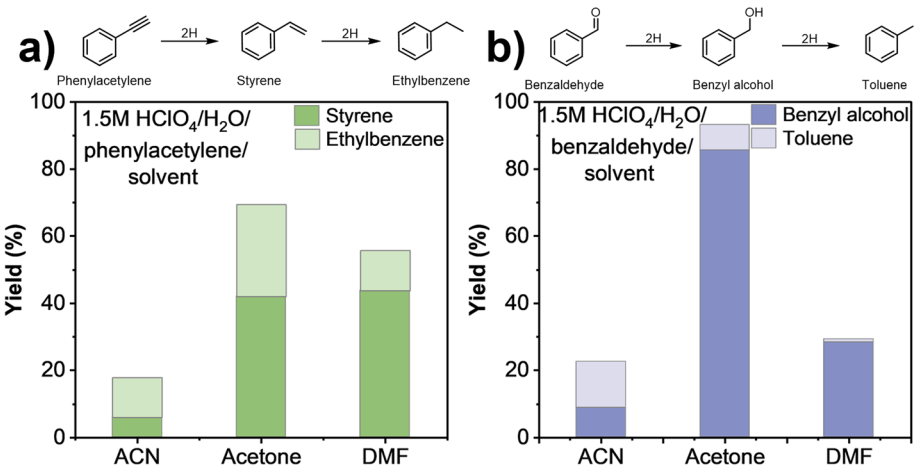

Fig. 3 The yield of electrochemical semihydrogenation of (a) phenylacetylene and (b) benzaldehyde at −1.1 V *vs.* RHE in 1.5 M $HClO_4$/H_2O/DMF hybrid electrolytes for 2 hours using Ni foam.

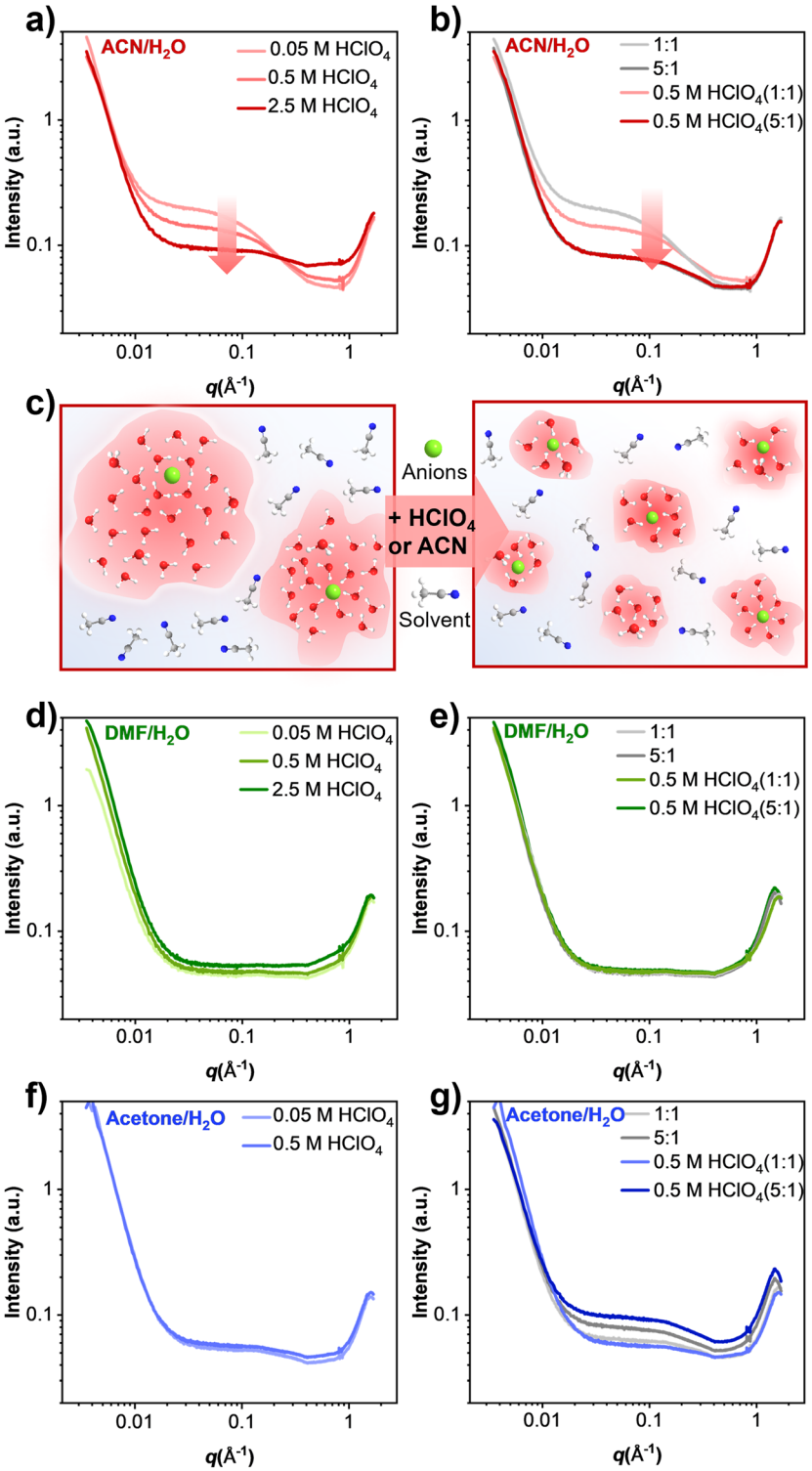

Fig. 4 (a) and (b) SAXS spectra recorded for ACN/water with different $HClO_4$ concentrations and volume ratios of ACN and water (1 : 1 and 5 : 1), respectively. (c) Scheme depicting the decrease in the size of the aqueous heterogeneities when increasing the acid concentration or the ACN to H_2O volume ratio. (d) and (e) SAXS spectra recorded for DMF/water mixtures with different $HClO_4$ concentrations and volume ratios of DMF and water (1 : 1 and 5 : 1), respectively. (f) and (g) SAXS spectra recorded for acetone/water mixtures with different $HClO_4$ concentrations and volume ratios of acetone and water (1 : 1 and 5 : 1), respectively.

the breakdown of tetrahedral water networks. Finally, by comparing the calibrated spectra of ACN/water and DMF/water mixtures (Fig. S12), contributions at higher wavenumbers are found to be predominant in ACN mixtures with an increase in free or single paired water molecules, confirming the weaker hydrogen bonding networks in ACN-based mixtures compared

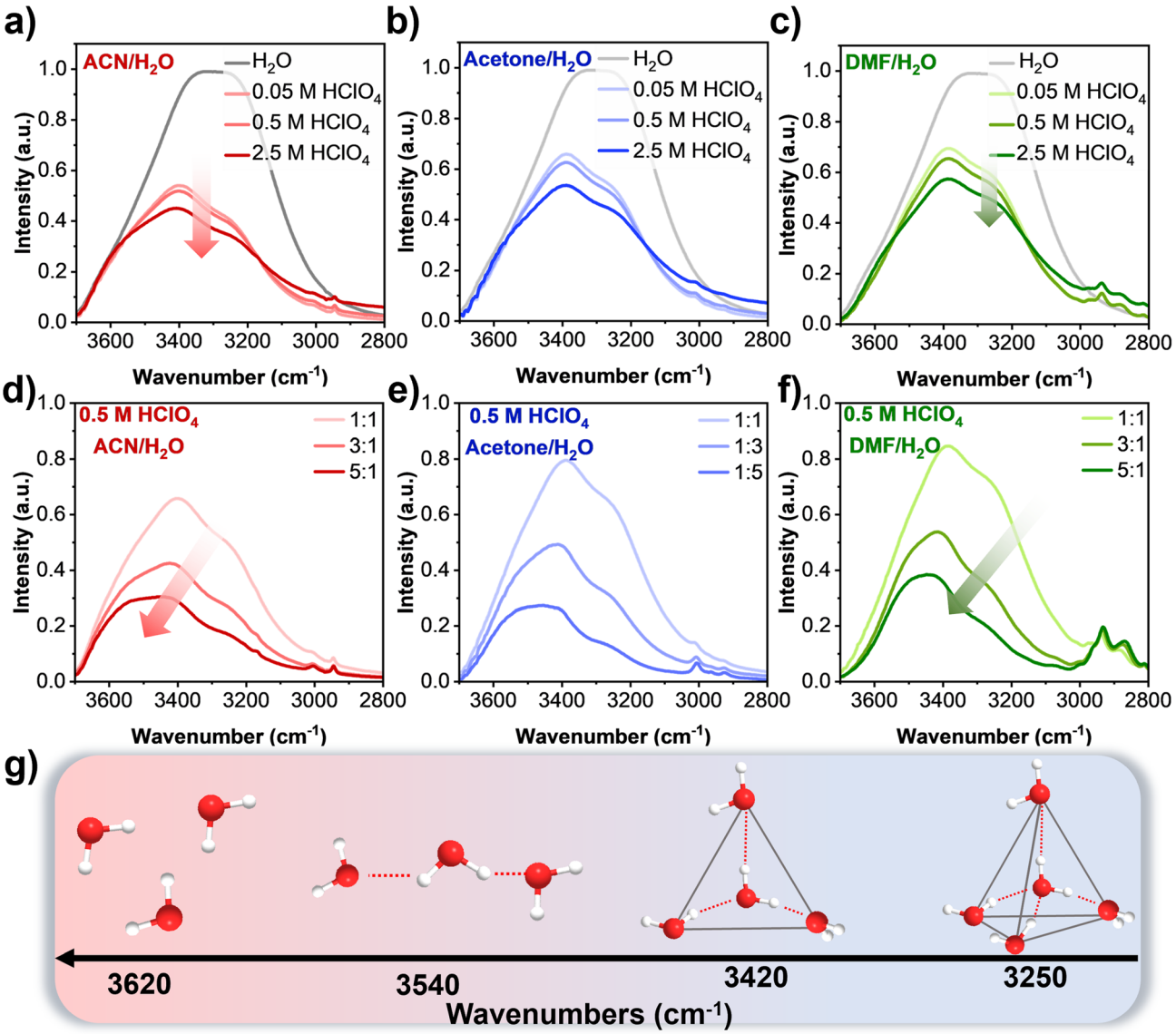

Fig. 5 (a)–(c) FTIR spectra of organic solvent/water mixtures with different $HClO_4$ concentrations. (d)–(f) FTIR spectra of 0.5 M $HClO_4$ organic solvent/water mixtures with different volume ratios of solvent and water (1 : 1, 3 : 1 and 5 : 1). (g) Scheme of the change in water structures with different electrolyte compositions.

to DMF ones. This conclusion is supported by observing that ΔH_{mix} for the ACN mixtures (mole fraction of water of 0.7387) is positive for the mole fractions studied in this work, while it is negative for DMF (mole fraction of 0.7987) mixtures with 0.5 M $HClO_4$.[59–62] When the amount of solvent increases, ΔH_{mix} for acetone/water mixtures shifts from negative to positive, explaining why acetone shows a similar trend to DMF with a large water amount while behaving like ACN with a small water amount, as can be seen from the IR spectra (Fig. 5d and f).

SAXS and IR spectra have confirmed the existence of aqueous heterogeneities in ACN/water mixtures, while acetone/water and DMF/water mixtures are homogeneous. Combined with the electrochemical results, we find that the yield of electrochemical hydrogenation of unsaturated hydrocarbons (alkynes) and of one representative aldehyde in ACN/water mixtures is always low, and we attribute this result to the presence of aqueous heterogeneities. We hypothesize that under negative polarization, the interface is rich in water, as a result of the presence of H^+ in the aqueous heterogeneities which are attracted to the interface, like what we previously observed for Li^+-containing hybrid electrolytes.[22,28] One can therefore conclude that a more aqueous-like interfacial solvation structure is detrimental for the hydrogenation reaction (Fig. 6a), likely due to the difficult access of the organic substrate to the interface which prevents its reactivity with protonated intermediates.[63] Therefore, for ACN-based mixtures, the semi-hydrogenation yield remains low independent of water or proton content. Instead, for DMF and acetone-based systems, the electrolytes are found to be homogeneous. Thus, both water and the organic substrate have easier access to the interface,

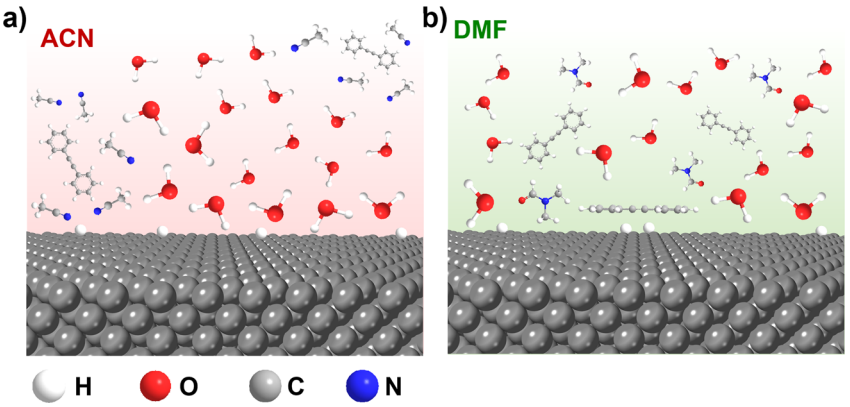

Fig. 6 Scheme of the interfacial environment in (a) ACN-based mixtures for which the interface is rich in water due to the accumulation of aqueous domains under negative polarization while for (b) DMF mixtures, the interface contains both water and the organic substrate.

and the semi-hydrogenation reaction can proceed (Fig. 6b). Hence, the yield in homogeneous hybrid electrolytes, *i.e.* acetone/water and DMF/water systems, is significantly higher. Moreover, the yield is affected in these systems by the acid concentration. Increasing the acid concentration increases the reactant for semi-hydrogenation and thus increases the yield, while at large concentrations the HER becomes dominant, explaining the optimum observed in Fig. 1b.

Conclusion

This study demonstrates that the yield for the semi-hydrogenation of unsaturated hydrocarbons depends on the composition of hybrid electrolytes, *i.e.* it can be tailored. First, we demonstrate that water does not serve as a proton source in hybrid electrolytes for this reaction. Instead, by measuring the yield for semi-hydrogenation in various electrolytes as a function of the acid concentration, we find that an optimum is obtained in DMF- and acetone-based mixtures with 1–1.5 M $HClO_4$. Comparing these results with the potential for the HER in these mixtures, we find that at concentrations greater than the optimum, the HER becomes predominant, while at low concentrations increasing the amount of acids increases the semi-hydrogenation yields by increasing the amount of reactants. A discrepancy is observed for ACN-based electrolyte for which the yield remains low independent of the acid concentration. Spectroscopic measurements were carried out to explain this stark difference. In ACN-based mixtures, aqueous heterogeneities were observed by SAXS, whose size decreases on increasing the acid concentration and/or decreasing water content. Instead, DMF- and acetone-based electrolytes show no sign of heterogeneities (DMF) or a very limited amount of heterogeneities (acetone). The FTIR spectroscopic results further reveal that $HClO_4$ addition induces weakening of the hydrogen bonding network, independent of the organic solvent; similar weakening is observed on decreasing the water content. By comparing the electrochemical results with the spectroscopic ones, we conclude that aqueous heterogeneities are detrimental for semi-hydrogenation reactions. Indeed, under negative polarization, the electrochemical interface becomes rich in water for systems showing heterogeneities, as a result of the presence of H^+ in the aqueous domains. This hydrophilicity of the interface hinders the reaction by limiting the organic substrate adsorption to interact with protonated intermediates that are formed by H^+ reduction; the yield thus remains low independent of the composition while the HER becomes more facile with the acid concentration. This work offers the necessary understanding to tailor the reaction environment for reactions including not only hydrogenation, but also deuteration or oxygenation reactions of organic substrates that also require the use of hybrid electrolytes. Nevertheless, substantial efforts are needed in the design of electrocatalysts to increase the faradaic efficiency (FE) and the efficiency of electrochemical semihydrogenation, which remains low due to the predominance of the HER (Fig. S13). Furthermore, future work should also be dedicated to understanding the effect of substrate/water interactions, with our results suggesting that it may play a significant role in the outcome of the reaction.

Experimental section

Reagents

Acetone, acetonitrile, and dimethylformamide (HPLC grade) were purchased from Fisher Scientific. Perchloric acid (70%), diphenylacetylene, phenylacetylene, and benzaldehyde were purchased from Sigma-Aldrich. Sulfuric acid (98%) was purchased from Oakwood. D-Chloroform (99.8% D) was purchased from Cambridge Isotope Laboratory. Milli-Q water (18.2 MΩ cm^{-1} at 25 °C) was used for electrolytes containing water.

Electrochemical measurements

Data were acquired on a BioLogic VSP potentiostat. All electrochemical measurements were performed using a three-electrode cell setup with a leakless Ag/AgCl reference electrode (ET069, diameter: 5 mm, L: 130 mm, eDAQ) with stirring under ambient conditions. A graphite rod was used as the counter electrode and placed in a compartment separated by a frit. All electrochemical measurements were conducted at room temperature. Prior to any measurements, commercial Ni

foam (from MSE) was immersed in a 0.5 M HCl solution for 5 min to remove any oxide layer and then washed with Milli-Q water and acetone several times. The ohmic drop was measured by electrochemical impedance spectroscopy (EIS) before and after electrochemical measurements and the values depended on the supporting salt concentration and the solvent. The ohmic drop compensation was performed in the cyclic voltammetry measurements (85% of correction).

The yield of *cis*-stilbene was calculated based on the below equation:

$$\text{Yield } (\%) = \frac{n_{cis\text{-stilbene}}}{n_{\text{diphenylacetylene(i)}}} \times 100\% \quad (1)$$

The faradaic efficiency (FE) was calculated according to the below equation:

$$\text{FE } (\%) = \frac{Z \times n_{cis\text{-stilbene}} \times F}{Q} \times 100\% \quad (2)$$

where Z is the number of electrons per molecule of the resultant product, F is the Faraday constant (96 485 C mol^{-1}), and Q is the total charge passed in the cell during the electrolysis process (coulombs, C).

The mole balance was calculated according to the below equation:[64,65]

$$\text{Mole balance } (\%) = \frac{n_{\text{diphenylacetylene(f)}} + n_{cis\text{-stilbene}} + n_{trans\text{-stilbene}} + n_{\text{dibenzyl}}}{n_{\text{diphenylacetylene(i)}}} \times 100\% \quad (3)$$

where the subscripts i and f refer to the initial and final amount of diphenylacetylene.

Reversible hydrogen electrode (RHE) measurements

A platinum rotating disk electrode (RDE from Pine Research) rotated at 1600 rpm was used to accurately measure the RHE equilibrium potential. RHE was determined by measuring the open circuit voltage (OCV) in the H_2-saturated electrolytes using the Pt RDE as a working electrode and a graphite rod as a reference electrode. The Pt electrode was polished with 0.1 μm and 0.03 μm polishing slurries and residual traces of slurries were removed by sonicating the as-polished electrodes in the water and acetone solutions three times. The polycrystalline platinum electrode was further electrochemically cleaned in 0.5 M sulfuric acid solution by 10 cycles of cyclic voltammetry (CV) between −0.25 and 1.25 V *vs.* leakless Ag/AgCl at 50 mV s^{-1}. Then the Pt electrode was rinsed with Milli-Q water and air-dried.

FTIR spectroscopy

ATR-FTIR spectra were acquired at 4 cm^{-1} with 64 scans using the diamond ATR crystal on a Bruker spectrometer.

Nuclear magnetic resonance spectroscopy

After 2 hours of reaction, the electrolyte was transferred into a flask and the product was extracted with methylene chloride twice. The product thus collected was dissolved in d-chloroform and liquid-state ^{1}H NMR spectra were recorded at 500 MHz on a Bruker AVANCE NEO spectrometer.

Small-angle X-ray scattering (SAXS)

Small-angle X-ray scattering experiments were performed at sector 12 ID-E of the Advanced Photon Source at Argonne National Laboratory. A Pilatus 2 M detector was located about 5 m downstream from the sample. The X-ray energy is 17.0 keV and exposure time is 1 s. The sample-to-detector distance was calibrated using the diffraction rings of a silver behenate ($AgC_{22}H_{43}O_2$) standard. The 2D scattering images collected using the detector were subsequently azimuthally averaged to 1D curves.

Author contributions

R. Z. and A. G. designed the experiments. R. Z. and X. L. collected and analyzed the data. All the authors edited the manuscript and discussed the scientific results.

Conflicts of interest

There are no conflicts to declare.

Data availability

The data supporting this article have been included as part of the SI.

Supplementary information is available. See DOI: https://doi.org/10.1039/d5sc03012a.

Acknowledgements

This work was supported by the donors of the ACS Petroleum Research Fund under the grant number 67977-DNI4. This research was supported by the NSF-MRI award CHE-2117246. This research was performed on APS beam time award(s) (https://doi.org/10.46936/APS-189135/60013531) from the Advanced Photon Source, a U.S. Department of Energy (DOE) Office of Science user facility at Argonne National Laboratory, and is based on research supported by the U.S. DOE Office of Science-Basic Energy Sciences, under Contract No. DE-AC02-06CH11357. T. Li is thankful for the support from NSF 2323117.

References

1 C. Zhu, N. W. Ang, T. H. Meyer, Y. Qiu and L. Ackermann, Organic electrochemistry: molecular syntheses with potential, *ACS Cent. Sci.*, 2021, **7**(3), 415–431.
2 Q. Jing and K. D. Moeller, From molecules to molecular surfaces. Exploiting the interplay between organic synthesis and electrochemistry, *Acc. Chem. Res.*, 2019, **53**(1), 135–143.
3 B. A. Frontana-Uribe, R. D. Little, J. G. Ibanez, A. Palma and R. Vasquez-Medrano, Organic electrosynthesis: a promising green methodology in organic chemistry, *Green Chem.*, 2010, **12**(12), 2099–2119.

4 E. J. Horn, B. R. Rosen and P. S. Baran, Synthetic organic electrochemistry: an enabling and innately sustainable method, *ACS Cent. Sci.*, 2016, **2**(5), 302–308.
5 J. Yang, H. Qin, K. Yan, X. Cheng and J. Wen, Advances in electrochemical hydrogenation since 2010, *Adv. Synth. Catal.*, 2021, **363**(24), 5407–5416.
6 X. Li, X. Wu, L. Tang, F. Xie and W. Zhang, Benzylamine as Hydrogen Transfer Agent: Cobalt-Catalyzed Chemoselective C═C Bond Reduction of β-Trifluoromethylated α,β-Unsaturated Ketones via 1,5-Hydrogen Transfer, *Chem.–Asian J.*, 2019, **14**(21), 3835–3839.
7 L. J. Murphy, M. J. Ferguson, R. McDonald, M. D. Lumsden and L. Turculet, Synthesis of Bis(phosphino)silyl Pincer-Supported Iron Hydrides for the Catalytic Hydrogenation of Alkenes, *Organometallics*, 2018, **37**(24), 4814–4826.
8 K. Tokmic, C. R. Markus, L. Zhu and A. R. Fout, Well-defined cobalt(I) dihydrogen catalyst: experimental evidence for a Co(I)/Co(III) redox process in olefin hydrogenation, *J. Am. Chem. Soc.*, 2016, **138**(36), 11907–11913.
9 N. Corbin, G. P. Junor, T. N. Ton, R. J. Baker and K. Manthiram, Toward improving the selectivity of organic halide electrocarboxylation with mechanistically informed solvent selection, *J. Am. Chem. Soc.*, 2023, **145**(3), 1740–1748.
10 B. Li and H. Ge, Highly selective electrochemical hydrogenation of alkynes: rapid construction of mechanochromic materials, *Sci. Adv.*, 2019, **5**(5), eaaw2774.
11 S. Wang, K. Uwakwe, L. Yu, J. Ye, Y. Zhu, J. Hu, R. Chen, Z. Zhang, Z. Zhou and J. Li, Highly efficient ethylene production via electrocatalytic hydrogenation of acetylene under mild conditions, *Nat. Commun.*, 2021, **12**(1), 7072.
12 Y. Wu, C. Liu, C. Wang, Y. Yu, Y. Shi and B. Zhang, Converting copper sulfide to copper with surface sulfur for electrocatalytic alkyne semi-hydrogenation with water, *Nat. Commun.*, 2021, **12**(1), 3881.
13 C. P. Andrieux, M. Robert and J.-M. Saveant, Role of environmental factors in the dynamics of intramolecular dissociative electron transfer. Effect of solvation and ion-pairing on cleavage rates of anion radicals, *J. Am. Chem. Soc.*, 1995, **117**(36), 9340–9346.
14 C. Han, J. Zenner, J. Johny, N. Kaeffer, A. Bordet and W. Leitner, Electrocatalytic hydrogenation of alkenes with Pd/carbon nanotubes at an oil–water interface, *Nat. Catal.*, 2022, **5**(12), 1110–1119.
15 Y. Gao, R. Yang, C. Wang, C. Liu, Y. Wu, H. Li and B. Zhang, Field-induced reagent concentration and sulfur adsorption enable efficient electrocatalytic semihydrogenation of alkynes, *Sci. Adv.*, 2022, **8**(8), eabm9477.
16 F. Chen, L. Li, C. Cheng, Y. Yu, B.-H. Zhao and B. Zhang, Ethylene electrosynthesis from low-concentrated acetylene via concave-surface enriched reactant and improved mass transfer, *Nat. Commun.*, 2024, **15**(1), 5914.
17 L. Wickert, K. Pellumbi, J. T. Kleinhaus, J. Wolf, K. junge Puring, D. Siegmund and U. P. Apfel, Effect of electrolyte composition and mass transport on electrochemical hydrogenations of a terminal alkynol, *Chem. Ing. Tech.*, 2024, **96**(5), 607–615.
18 Y. Zhao, J. Wang, X. Zha, X. Sheng, L. Dong, X. P. Wu, Z. Liu, H. Jiang and C. Li, A Cosolvent Electrolyte Boosting Electrochemical Alkynol Semihydrogenation, *J. Am. Chem. Soc.*, 2025, **147**(2), 1938–1947.
19 A. Valiente, P. Martínez-Pardo, G. Kaur, M. J. Johansson and B. Martín-Matute, Electrochemical Proton Reduction over Nickel Foam for Z-Stereoselective Semihydrogenation/deuteration of Functionalized Alkynes, *ChemSusChem*, 2022, **15**(1), e202102221.
20 P. J. Tortajada, T. Kärnman, P. Martínez-Pardo, C. Nilsson, H. Holmquist, M. J. Johansson and B. Martín-Matute, Electrochemical hydrogenation of alkenes over a nickel foam guided by life cycle, safety and toxicological assessments, *Green Chem.*, 2025, **27**(1), 227–239.
21 S. Kolb and D. B. Werz, Site-selective Hydrogenation/Deuteration of Benzylic Olefins Enabled by Electroreduction Using Water, *Chem.–Eur. J.*, 2023, **29**(32), e202300849.
22 N. Dubouis, A. Serva, R. Berthin, G. Jeanmairet, B. Porcheron, E. Salager, M. Salanne and A. Grimaud, Tuning water reduction through controlled nanoconfinement within an organic liquid matrix, *Nat. Catal.*, 2020, **3**(8), 656–663.
23 P. Li, C. Guo, S. Wang, D. Ma, T. Feng, Y. Wang and Y. Qiu, Facile and general electrochemical deuteration of unactivated alkyl halides, *Nat. Commun.*, 2022, **13**(1), 3774.
24 P. L. Norcott, Current electrochemical approaches to selective deuteration, *Chem. Commun.*, 2022, **58**(18), 2944–2953.
25 C. Liu, F. Chen, B.-H. Zhao, Y. Wu and B. Zhang, Electrochemical hydrogenation and oxidation of organic species involving water, *Nat. Rev. Chem.*, 2024, **8**(4), 277–293.
26 A. Serva, N. Dubouis, A. Grimaud and M. Salanne, Confining water in ionic and organic solvents to tune its adsorption and reactivity at electrified interfaces, *Acc. Chem. Res.*, 2021, **54**(4), 1034–1042.
27 F. Dorchies, A. Serva, A. Sidos, L. Michot, M. Deschamps, M. Salanne and A. Grimaud, Correlating Substrate Reactivity at Electrified Interfaces with the Electrolyte Structure in Synthetically Relevant Organic Solvent/Water Mixtures, *J. Am. Chem. Soc.*, 2024, **146**(25), 17495–17507.
28 F. Dorchies, A. Serva, D. Crevel, J. De Freitas, N. Kostopoulos, M. Robert, O. Sel, M. Salanne and A. Grimaud, Controlling the Hydrophilicity of the Electrochemical Interface to Modulate the Oxygen-Atom Transfer in Electrocatalytic Epoxidation Reactions, *J. Am. Chem. Soc.*, 2022, **144**(49), 22734–22746.
29 V. Koverga, Á. Juhász, D. Dudariev, M. Lebedev, A. Idrissi and P. Jedlovszky, Local Structure of DMF–Water Mixtures, as Seen from Computer Simulations and Voronoi Analysis, *J. Phys. Chem. B*, 2022, **126**(36), 6964–6978.
30 X. Liu, S. Wang, X. Xu, H. Khair, Z. Dong, H. Wang, W. Zhang, T. Yu, Z. Men and C. Sun, Exploring the dynamic changes in hydrogen bond structure of water and heavy water under external perturbation of DMF, *Spectrochim. Acta, Part A*, 2024, **305**, 123493.

31 D. Tomar, B. Rana and K. C. Jena, The structure of water–DMF binary mixtures probed by linear and nonlinear vibrational spectroscopy, *J. Chem. Phys.*, 2020, **152**(11), 114707.
32 N. S. Venkataramanan, Cooperativity of intermolecular hydrogen bonds in microsolvated DMSO and DMF clusters: a DFT, AIM, and NCI analysis, *J. Mol. Model.*, 2016, **22**, 1–11.
33 N. Huang, D. Nordlund, C. Huang, U. Bergmann, T. M. Weiss, L. G. Pettersson and A. Nilsson, X-ray Raman scattering provides evidence for interfacial acetonitrile-water dipole interactions in aqueous solutions, *J. Chem. Phys.*, 2011, **135**(16), 164509.
34 Y. Marcus, The structure of and interactions in binary acetonitrile + water mixtures, *J. Phys. Org. Chem.*, 2012, **25**(12), 1072–1085.
35 M. Nagasaka, H. Yuzawa and N. Kosugi, Microheterogeneity in aqueous acetonitrile solution probed by soft X-ray absorption spectroscopy, *J. Phys. Chem. B*, 2020, **124**(7), 1259–1265.
36 T. Takamuku, Y. Noguchi, M. Matsugami, H. Iwase, T. Otomo and M. Nagao, Heterogeneity of acetonitrile–water mixtures in the temperature range 279–307 K studied by small-angle neutron scattering technique, *J. Mol. Liq.*, 2007, **136**(1–2), 147–155.
37 T. Takamuku, M. Tabata, A. Yamaguchi, J. Nishimoto, M. Kumamoto, H. Wakita and T. Yamaguchi, Liquid structure of acetonitrile–water mixtures by X-ray diffraction and infrared spectroscopy, *J. Phys. Chem. B*, 1998, **102**(44), 8880–8888.
38 J.-M. McGregor, J. T. Bender, A. S. Petersen and J. Resasco, Organic electrolyte cations promote non-aqueous CO_2 reduction by mediating interfacial electric fields, *Nat. Catal.*, 2025, **8**(1), 79–91.
39 G. Cassone, F. Creazzo, P. V. Giaquinta, J. Sponer and F. Saija, Ionic diffusion and proton transfer in aqueous solutions of alkali metal salts, *Phys. Chem. Chem. Phys.*, 2017, **19**(31), 20420–20429.
40 E. Liu, J. Li, L. Jiao, H. T. T. Doan, Z. Liu, Z. Zhao, Y. Huang, K. Abraham, S. Mukerjee and Q. Jia, Unifying the hydrogen evolution and oxidation reactions kinetics in base by identifying the catalytic roles of hydroxyl-water-cation adducts, *J. Am. Chem. Soc.*, 2019, **141**(7), 3232–3239.
41 R. Iwata, L. Zhang, K. L. Wilke, S. Gong, M. He, B. M. Gallant and E. N. Wang, Bubble growth and departure modes on wettable/non-wettable porous foams in alkaline water splitting, *Joule*, 2021, **5**(4), 887–900.
42 N. Dubouis and A. Grimaud, The hydrogen evolution reaction: from material to interfacial descriptors, *Chem. Sci.*, 2019, **10**(40), 9165–9181.
43 N. Dubouis, A. Serva, E. Salager, M. Deschamps, M. Salanne and A. Grimaud, The fate of water at the electrochemical interfaces: electrochemical behavior of free water versus coordinating water, *J. Phys. Chem. Lett.*, 2018, **9**(23), 6683–6688.
44 M. F. Suárez-Herrera, M. Costa-Figueiredo and J. M. Feliu, Voltammetry of basal plane platinum electrodes in acetonitrile electrolytes: effect of the presence of water, *Langmuir*, 2012, **28**(11), 5286–5294.
45 I. Ledezma-Yanez, O. Díaz-Morales, M. C. Figueiredo and M. T. Koper, Hydrogen oxidation and hydrogen evolution on a platinum electrode in acetonitrile, *ChemElectroChem*, 2015, **2**(10), 1612–1622.
46 I. Ledezma-Yanez and M. T. Koper, Influence of water on the hydrogen evolution reaction on a gold electrode in acetonitrile solution, *J. Electroanal. Chem.*, 2017, **793**, 18–24.
47 S. Nogami, N. Shida, S. Iguchi, K. Nagasawa, H. Inoue, I. Yamanaka, S. Mitsushima and M. Atobe, Mechanistic insights into the electrocatalytic hydrogenation of alkynes on Pt–Pd electrocatalysts in a proton-exchange membrane reactor, *ACS Catal.*, 2022, **12**(9), 5430–5440.
48 G. Han, G. Li and Y. Sun, Electrocatalytic hydrogenation using palladium membrane reactors, *JACS Au*, 2024, **4**(2), 328–343.
49 R. S. Sherbo, A. Kurimoto, C. M. Brown and C. P. Berlinguette, Efficient electrocatalytic hydrogenation with a palladium membrane reactor, *J. Am. Chem. Soc.*, 2019, **141**(19), 7815–7821.
50 H. Chen, J. Iyer, Y. Liu, S. Krebs, F. Deng, A. Jentys, D. J. Searles, M. A. Haider, R. Khare and J. A. Lercher, Mechanism of electrocatalytic H_2 evolution, carbonyl hydrogenation, and carbon–carbon coupling on Cu, *J. Am. Chem. Soc.*, 2024, **146**(20), 13949–13961.
51 G. Cheng, A. Jentys, O. Y. Gutiérrez, Y. Liu, Y.-H. Chin and J. A. Lercher, Critical role of solvent-modulated hydrogen-binding strength in the catalytic hydrogenation of benzaldehyde on palladium, *Nat. Catal.*, 2021, **4**(11), 976–985.
52 U. Sanyal, S. F. Yuk, K. Koh, M. S. Lee, K. Stoerzinger, D. Zhang, L. C. Meyer, J. A. Lopez-Ruiz, A. Karkamkar and J. D. Holladay, Hydrogen bonding enhances the electrochemical hydrogenation of benzaldehyde in the aqueous phase, *Angew. Chem.*, 2021, **133**(1), 294–300.
53 X. Liu, L. Fang, X. Lyu, R. E. Winans and T. Li, Unveiling the liquid electrolyte solvation structure by small angle X-ray scattering, *Chem. Mater.*, 2023, **35**(23), 9821–9832.
54 K. Qian, R. E. Winans and T. Li, Insights into the nanostructure, solvation, and dynamics of liquid electrolytes through small-angle X-ray scattering, *Adv. Energy Mater.*, 2021, **11**(4), 2002821.
55 X. Liu, S.-C. Lee, S. Seifert, R. E. Winans and T. Li, Relationship of the Molecular Structure and Transport Properties of Imide-Based Lithium Salts of "Acetonitrile/Water-in-Salt" Electrolytes, *Chem. Mater.*, 2023, **35**(16), 6415–6422.
56 Y. Chen, Y.-H. Zhang and L.-J. Zhao, ATR-FTIR spectroscopic studies on aqueous $LiClO_4$, $NaClO_4$, and $Mg(ClO_4)_2$ solutions, *Phys. Chem. Chem. Phys.*, 2004, **6**(3), 537–542.
57 R. Khatib, E. H. Backus, M. Bonn, M.-J. Perez-Haro, M.-P. Gaigeot and M. Sulpizi, Water orientation and hydrogen-bond structure at the fluorite/water interface, *Sci. Rep.*, 2016, **6**(1), 24287.

58 D. M. Carey and G. M. Korenowski, Measurement of the Raman spectrum of liquid water, *J. Chem. Phys.*, 1998, **108**(7), 2669–2675.
59 A. V. Benedetti, M. Cilense, D. Vollet and R. Montone, Thermodynamic properties of liquid mixtures. III. Acetone–water, *Thermochim. Acta*, 1983, **66**(1–3), 219–223.
60 M. Cilense, A. V. Benedetti and D. Vollet, Thermodynamic properties of liquid mixtures. II. Dimethylformamide-water, *Thermochim. Acta*, 1983, **63**(2), 151–156.
61 K. Morcom and R. Smith, Enthalpies of mixing of water + methyl cyanide, *J. Chem. Thermodyn.*, 1969, **1**(5), 503–505.
62 M. Matsumoto, H. Tanaka and K. Nakanishi, Acetonitrile pair formation in aqueous solution, *J. Chem. Phys.*, 1993, **99**(9), 6935–6940.
63 B. Chen, M. S. Wijesinghe, A. Grimaud and M. M. Waegele, Investigating the Electric Double-Layer Structures between a Pt Electrode and Water/Acetonitrile Hybrid Electrolytes, *J. Phys. Chem. Lett.*, 2025, **16**(7), 1779–1786.
64 S. Jung and E. J. Biddinger, Electrocatalytic hydrogenation and hydrogenolysis of furfural and the impact of homogeneous side reactions of furanic compounds in acidic electrolytes, *ACS Sustain. Chem. Eng.*, 2016, **4**(12), 6500–6508.
65 S. Jung and E. J. Biddinger, Controlling competitive side reactions in the electrochemical upgrading of furfural to biofuel, *Energy Technol.*, 2018, **6**(7), 1370–1379.